Theory of nonspecular tunneling through magnetic tunnel junctions

X.-G. Zhang*
Center for Nanophase Materials Sciences and Computer Science and Mathematics Division, Oak Ridge National Laboratory, Oak Ridge, Tennessee 37831-6493, USA

Yan Wang and X. F. Han
State Key Laboratory of Magnetism, Beijing National Laboratory for Condensed Matter Physics, Institute of Physics, Chinese Academy of Science, Beijing 100080, People's Republic of China
(Received 2 January 2008; published 29 April 2008)

We derive a simple formalism of vertex corrections for the tunneling probability of an electron due to nonspecular scattering. Predictions of the model in terms of the barrier thickness dependence of the resistance and oscillatory tunneling magnetoresistance (TMR) are in excellent agreement with experiment. We show that the TMR is directly linked to the vertex corrections. Thus, reducing the nonspecular scattering within the barrier layer is crucial for increasing the TMR. Applying this model to the analysis of the temperature dependence of TMR yields a temperature dependent interface scattering rate.

DOI: 10.1103/PhysRevB.77.144431 PACS number(s): 72.25.Mk, 73.40.Gk, 73.40.Rw, 75.70.Cn

I. INTRODUCTION

Magnetic tunnel junctions consisting of ferromagnet electrodes and an insulating barrier are a special type of tunnel junctions extensively studied for their tunneling magnetoresistance (TMR) effect.[1–6] The two spin channels in a magnetic tunnel junction, usually called the majority- and the minority-spin channels as determined by the electron spin directions in the electrodes, contribute different tunneling currents and can be manipulated by applying an external magnetic field. This feature leads to giant tunneling magnetoresistance[4–6] and have significant technological implications.

In this paper, we exploit this feature of magnetic tunnel junctions to study the details of tunneling process not accessible in nonmagnetic tunnel junctions, in particular, the nonspecular ($\mathbf{k}_\parallel$ nonconserving) scattering inside the tunnel barrier and on the barrier-electrode interfaces. Traditional models[4,7,8] of tunnel junctions of planar geometry all assume specular transmission, i.e., that the electron momentum parallel to the junction plane, $\mathbf{k}_\parallel$, is always conserved in the tunneling process. Vertex corrections due to impurity or defect scattering inside the barrier layer have only been considered for specific scattering events.[9] No general theory has been developed for the vertex corrections.

Here, we present a simple linear model for the vertex corrections. This model will help solve two of the longstanding puzzles in the study of magnetic tunnel junctions. One is the discrepancy between theory and experiment on the thickness dependence of the TMR. The theory[4] predicts an increase of the TMR with the barrier thickness because the antiparallel resistance R_{AP} increases faster with the barrier thickness than the parallel resistance R_P. Experiments show that the two resistances increase at the same rate with the barrier thickness so the TMR is essentially a constant. The second puzzle is the source of the oscillatory TMR[6,10] as a function of barrier thickness. By using our model, we show that in the presence of vertex corrections, conduction through all tunneling channels decreases with the barrier thickness at the same rate as the dominant channel. The interference term also decreases at this rate. By combining with the first-principles calculations, we obtain excellent agreement with recent measurements of the barrier thickness dependence of the resistance, TMR, and the resistance oscillation. By using our model, we also extract a temperature dependence of the interface scattering rate from measurements of epitaxial junctions.[5,11]

We first compare the experimental results to first-principles calculations without including any defect scattering in Sec. II, which highlights the discrepancies discussed above. In Sec. III, we derive the master equation for our model. The master equation is then used to study the thickness dependence of the resistance in Sec. IV, the interference of evanescent waves and oscillatory TMR in Sec. V, and, finally, the interface scattering and the temperature dependence in Sec. VI.

II. BARRIER THICKNESS DEPENDENCE WITHOUT DEFECT SCATTERING

Before we present the theoretical model for nonspecular tunneling, let us first examine the first-principles theory for specular tunneling in the absence of any defect scattering. This serves two purposes. First, by comparing the first-principles results with experimental measurements, it motivates the subsequent model for diffuse scattering. Second, the first-principles calculation will also produce parameters that will be used later in the new model.

The first-principles calculation uses the layer Korringa–Kohn–Rostoker (layer KKR) code.[12] In this calculation, the electrode layers of Fe are fixed at the experimental lattice constant of 2.866 Å and the in-plane MgO lattice constant (along the [100] axis) is $\sqrt{2}$ times larger or 4.053 Å. The out-of-plane MgO lattice spacing (along [001]) is 2.21 Å, which is the experimental value.[6] The Fe-O distance, atomic spheres, and the empty sphere in the interfacial Fe layer are the same as in Ref. 4.

First, we calculate the complex band structure at the Fermi energy of the Fe electrodes for a bulk MgO lattice built by using the self-consistent potential of the middle MgO layer of a Fe/6MgO/Fe tunnel junction. The complex

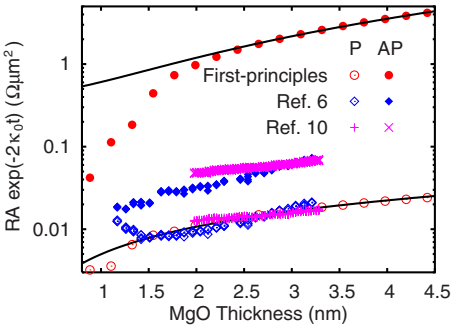

FIG. 1. (Color online) Sheet resistance of an Fe/MgO/Fe tunnel junction as a function of MgO thickness t scaled by $\exp(-2\kappa_0 t)$. First-principles calculation (open red circle, R_P; filled red circle, R_{AP}) is compared to two experiments (open blue diamond, R_P from Ref. 6; filled blue diamond, R_{AP} from Ref. 6; magenta plus, R_P from Ref. 10; magenta cross, R_{AP} from Ref. 10). The solid curves are fits to first-principles results using Eqs. (2) and (4).

band calculation yields $\kappa_0=2.92$ nm^{-1} for the Δ_1 band at $\mathbf{k}_\parallel=0$. This number will be used as the base line decay rate of the tunnel wave functions in the analysis below.

The total tunneling conductance of the Fe/MgO/Fe tunnel junction is calculated for both P (Fe electrode moments aligned parallel to each other) and AP (Fe electrode moments aligned antiparallel to each other) configurations for MgO thicknesses from 4 atomic layers up to 20 atomic layers. The integration over $\mathbf{k}_\parallel$ uses 8256 k points in 1/8 of the two-dimensional Brillouin zone (2DBZ). The results in terms of the sheet resistance as a function of MgO thickness t are plotted in Fig. 1. In this plot, the base line exponential factor $\exp(2\kappa_0 t)$ is removed from all data sets in order to facilitate a detailed comparison.

It is clear that neither R_P nor R_{AP} depends on the MgO thickness as a simple exponential. This result is consistent with a previous work.[13] To understand this, we invoke a simple model[14] of an isotropic complex band at the $\bar{\Gamma}$ point, which gives the conductance for each spin channel in the form,

$$G = \gamma A \frac{e^2}{h}\frac{1}{(2\pi)^2}\int_0^\infty e^{-2t\sqrt{k_\parallel^2+\kappa_0^2}} 2\pi k_\parallel dk_\parallel, \tag{1}$$

where A is the area of the sample and γ is a parameter determined by the metal electrodes and the contact. This equation directly works for the majority-spin channel in R_P. By neglecting the contribution from the minority-spin channel, we find

$$R_P A = \frac{8\pi h}{\gamma_P e^2}\frac{e^{2\kappa_0 t}}{\frac{1}{t^2}+\frac{2\kappa_0}{t}}. \tag{2}$$

By using γ_P as the only fitting parameter, this result fits the first-principles calculation of R_P very well, as shown in Fig. 1, except for the first two points where the minority-spin channel still contributes significantly to the total conductance.

For the AP configuration, because the Δ_1 band at $\bar{\Gamma}$ point cannot enter the opposite electrode, we modify the contribution to the conductance from $\mathbf{k}_\parallel$ by a factor of $1-\exp(-k_\parallel^2 d)$,

$$G_{AP} = \gamma_{AP} A \frac{e^2}{h}\frac{1}{(2\pi)^2}\int_0^\infty e^{-2t\sqrt{k_\parallel^2+\kappa_0^2}}(1-e^{-k_\parallel^2 d}) 2\pi k_\parallel dk_\parallel. \tag{3}$$

By integrating and assuming that $\kappa_0^2 d \gg 1$, we find

$$R_{AP}A = \frac{4\pi h}{\gamma_{AP}e^2}\frac{t^2+\kappa_0 d}{\kappa_0^2 d}e^{2\kappa_0 t}. \tag{4}$$

With two fitting parameters γ_{AP} and d, this fits the first-principles calculation of R_{AP} very well for large MgO thicknesses. At small thicknesses, the disagreement comes from the interface resonance states that significantly contribute to the AP conductance for thin MgO barriers.

The first-principles results are compared to two experiments in Fig. 1. The agreement for R_P is surprisingly good, especially considering that there are no adjustable parameters in the first-principles calculation. This agreement demonstrates two points. First, the nonspecular scattering seems to have little effect on R_P. This may be fortuitous and will be discussed in more detail in later sections. Second, the local density approximation (LDA) produces decay wave vectors at the Fermi energy that are in excellent agreement with experiments. In other words, the band gap error in the LDA does not affect the calculated tunneling current in the linear response regime. This is consistent with an earlier result.[14] The significantly larger resistance in experimental measured samples for MgO thickness smaller than 1.5 nm is due to increased diffusive scattering rates in these samples, as we will show in later sections.

The experiments disagree with the first-principles calculation of R_{AP} by more than an order of magnitude. This difference arises from diffusive scattering from defects inside the barrier and is not included in the first-principles calculation. We will develop a model for this type of scattering in the next section.

III. DERIVATION OF THE MASTER EQUATION

Our starting point is a crystalline epitaxial magnetic tunnel junction. The effect of defect scattering is introduced through scattering terms into the steady-state equation of motion, a master equation, for the electron density. This master equation is derived as the following. A specular tunneling wave function at the Fermi energy within the barrier region $0<z<t$, where t is the barrier thickness, takes the form,

$$\phi(\mathbf{r}) = \sum_n C_n \phi_n(\mathbf{r}), \tag{5}$$

for $\mathbf{r}=(x,y,z)$ and where $\phi_n(\mathbf{r})$ is the wave function of a single tunneling channel labeled by n, which includes both the transverse wave vector $\mathbf{k}_\parallel$ and the band labels. The forward tunneling wave function $\phi_n(\mathbf{r})$ is

$$\phi_n(\mathbf{r}) = \chi_n(x,y)[e^{-\kappa_n z} + B_n e^{\kappa_n (z-t)}], \tag{6}$$

where the weak oscillatory dependence of $\chi_n(x,y)$ on z on the atomic scale is omitted, κ_n is the decay wave vector, and

t is the thickness of the barrier. The backward tunneling wave function for the same channel is

$$\bar{\phi}_n(\mathbf{r}) = \chi_n(x,y)[e^{\kappa_n(z-t)} + \bar{B}_n e^{-\kappa_n z}]. \tag{7}$$

The wave functions of different channels are orthogonal, $\int \chi_n^*(x,y)\chi_{n'}(x,y)dxdy = A\delta_{nn'}$, where A is the area of the sample. The linear density of the tunneling electron at the Fermi energy is

$$\rho(z) = \frac{1}{A}\int |\phi(\mathbf{r})|^2 dxdy = \sum_n |C_n|^2 |e^{-\kappa_n z} + B_n e^{\kappa_n(z-t)}|^2. \tag{8}$$

With diffuse scattering, the coefficients C_n become z dependent. In addition, there is also a diffusive reflection contribution. We have

$$\rho(z) = \sum_n \rho_n(z) + \sum_n \bar{\rho}_n(z), \tag{9}$$

where the electron density for a single tunneling channel n is defined as

$$\rho_n(z) = \langle |C_n(z)|^2 \rangle |e^{-\kappa_n z} + B_n e^{\kappa_n(z-t)}|^2, \tag{10}$$

and where the angle bracket indicates a configurational average over the impurity scattering. Note that in Eqs. (9) and (10), the phases of the coefficients $C_n(z)$ do not affect the charge density.

To derive the master equation for $\rho_n(z)$, we consider a distribution of randomly placed point scatterers, similar to the model of free electrons with random point scatterers,[15] within a thin slice of space between planes $z=z_0$ and $z=z_1 = z_0+\delta$ inside a thick barrier. The scatterers are described by the random scattering potentials $V_m\delta(\mathbf{r}-\mathbf{r}_m)$. Later, we will invoke a configurational average such that

$$\langle V_m \rangle = 0 \tag{11}$$

and

$$\langle V_m V_{m'} \rangle = V^2 \delta_{mm'}. \tag{12}$$

We write the total wave function as

$$\psi(\mathbf{r}) = \sum_n C_n(z)\phi_n(\mathbf{r}) + \sum_n \bar{C}_n(z)\bar{\phi}_n(\mathbf{r}). \tag{13}$$

The relative phase factors in $C_n(z)$ between different tunneling channels will be randomized through the configurational average. This average also yields Eq. (9) from $\rho(z) = \frac{1}{A}\int \langle |\psi(\mathbf{r})|^2 \rangle dxdy$. The effects of the random point scatterers are expressed through the Lippmann–Schwinger equation,

$$\psi(\mathbf{r}) = \psi^{(0)}(\mathbf{r}) + \sum_{z_0<z_m<z_1} G^{(0)}(\mathbf{r},\mathbf{r}_m)V_m\psi(\mathbf{r}_m), \tag{14}$$

where the superscript (0) denotes the wave function and the Green's function when there are no scatterers between $z_0 < z < z_1$. Note that $\psi^{(0)}$ and $G^{(0)}$ still contain effects of scattering by defects inside the barrier but outside the thin slice of space $z_0 < z < z_1$ that we have cut out. For $\psi^{(0)}$, the coefficients $C_n^{(0)}$ and $\bar{C}_n^{(0)}$ are constants of z,

$$\psi^{(0)}(\mathbf{r}) = \sum_n C_n^{(0)}\phi_n(\mathbf{r}) + \sum_n \bar{C}_n^{(0)}\bar{\phi}_n(\mathbf{r}). \tag{15}$$

The retarded Green's function can be written in terms of an expansion by using the forward (ϕ_n) and backward ($\bar{\phi}_n$) tunneling wave functions,

$$G^{(0)}(\mathbf{r},\mathbf{r}') = \begin{cases} \sum_n S_n \bar{\phi}_n(\mathbf{r})\phi_n(\mathbf{r}'), & z < z' \\ \sum_n S_n \bar{\phi}_n(\mathbf{r}')\phi_n(\mathbf{r}), & z > z', \end{cases} \tag{16}$$

where S_n are constants to ensure the proper normalization of the singularities in the Green's function. In one dimension, the coefficient S_n is the inverse of the Wronskian between the two basis functions, and is independent of the position z at which the Wronskian is calculated. In particular, we note that when the two basis functions are both propagating waves, $S_n = 2ikt_n$, where t_n is the transmission amplitude, and for real t_n, S_n is imaginary. The total wave function is

$$\psi(\mathbf{r}) = \psi^{(0)}(\mathbf{r}) + \sum_n S_n\bar{\phi}_n(\mathbf{r}) \sum_{z<z_m<z_1} \phi_n(\mathbf{r}_m)V_m\psi(\mathbf{r}_m) + \sum_n S_n\phi_n(\mathbf{r}) \sum_{z_0<z_m<z} \bar{\phi}_n(\mathbf{r}_m)V_m\psi(\mathbf{r}_m). \tag{17}$$

We first consider the specular part of the wave function, i.e., the wave function including only the "scatter-out" contribution. For this purpose, Eq. (17) can be applied to the wave functions of individual channels, $\psi_n(\mathbf{r})$. We assume the case of thick barriers for which the transmission $T \ll 1$; therefore, $B_n \ll 1$ and the reflected waves in Eq. (6) can been omitted. Consequently, the second term on the right hand side of Eq. (17) is a higher order term of δ and therefore can also be dropped. Thus, at $z=z_0$, we have $\psi_n(x,y,z_0) = \psi_n^{(0)}(x,y,z_0)$. At $z=z_1$, we take the configurational average over the wave function, keeping the second order terms in V, and find

$$\langle \psi_n(\mathbf{r}) \rangle = \psi_n^{(0)}(\mathbf{r}) + V^2 \sum_{n'n''} S_{n'}S_{n''}\phi_{n'}(\mathbf{r}) \sum_{z_0<z_m<z} \bar{\phi}_{n'}(\mathbf{r}_m) \times \phi_{n''}(\mathbf{r}_m)\bar{\phi}_{n''}(\mathbf{r}_m)\psi_n^{(0)}(\mathbf{r}_m). \tag{18}$$

In the limit of $\delta \to 0$, this leads to a scatter-out term for the density,

$$\frac{d\rho_n(z)}{dz} = -(2\kappa_n + P_n)\rho_n(z), \tag{19}$$

where

$$P_n = -\frac{2V^2}{A}\,\mathrm{Re}\sum_{n'} S_n S_{n'} e^{-(\kappa_n+\kappa_{n'})t}\int \chi_n^2(x,y)\chi_{n'}^2(x,y)dxdy, \tag{20}$$

and we used $\rho_n(z_0) = \rho_n^{(0)}(z_0)$. We also replaced the summation over m by a volume integral. Because δ is small, the integration over z simply yields a factor of δ. Note that S_n, as normalization constants in Eq. (16), contain exponential thickness dependences such that $S_n e^{-\kappa_n t}$ should be independent of thickness. P_n is usually positive. This is certainly true in one dimension when S_n is imaginary. There are cases

where P_n can be negative. These correspond to resonant tunneling through impurities and are not considered here. Therefore, below, we will limit our discussion to positive P_n.

To derive the "scatter-in" contribution, i.e., the vertex corrections, we cannot use the Lippmann–Schwinger equation for individual channels. The total wave function, however, still satisfies the Lippmann–Schwinger equation [Eq. (17)]. Again, at $z=z_0$, $\psi_n(x,y,z_0)=\psi_n^{(0)}(x,y,z_0)$ and thus $\rho_n(z_0)=\rho_n^{(0)}(z_0)$. At $z=z_1$,

$$\psi(x,y,z_1)=\psi^{(0)}(x,y,z_1)+\sum_n S_n\phi_n(x,y,z_1)\sum_{z_0<z_m<z_1}\bar{\phi}_n(\mathbf{r}_m)V_m\psi(\mathbf{r}_m). \tag{21}$$

The equation for the density, keeping the second order terms in V, is given by

$$\rho(z_1)=\rho^{(0)}(z_1)+\frac{V^2}{A}\sum_n|S_n|^2\int|\phi_n(x,y,z_1)|^2dxdy\times\sum_{z_0<z_m<z_1}|\bar{\phi}_n(\mathbf{r}_m)\psi^{(0)}(\mathbf{r}_m)|^2+\frac{2V^2}{A}\times\mathrm{Re}\sum_{nn'}S_nS_{n'}\int\psi^{(0)*}(x,y,z_1)\phi_n(x,y,z_1)dxdy\times\sum_{z_0<z_m<z_1}\bar{\phi}_n(\mathbf{r}_m)\bar{\phi}_{n'}(\mathbf{r}_m)\phi_{n'}(\mathbf{r}_m)\psi^{(0)}(\mathbf{r}_m). \tag{22}$$

For small δ, this can be rewritten as

$$\rho_n(z_1)=\rho_n^{(0)}(z_1)+\sum_{n'}\rho_{n'}^{(0)}(z_1)P_{nn'}\delta-\rho_n^{(0)}(z_1)P_n\delta, \tag{23}$$

where

$$P_{nn'}=|S_n|^2e^{-2\kappa_{n'}t}\frac{V^2}{A}\int|\chi_n(x,y)\chi_{n'}(x,y)|^2dxdy. \tag{24}$$

This result contains both the scatter-out and the scatter-in terms. For $n\neq n'$, $P_{nn'}$ represents the scattering probability (per unit distance) from the state n' to state n (the scatter-in contribution) and is clearly positive definite. Taking the limit of $\delta\to 0$, we obtain the master equation,

$$\frac{d\rho_n(z)}{dz}=-(2\kappa_n+P_n)\rho_n(z)+\sum_{n'\neq n}P_{nn'}\rho_{n'}(z), \tag{25}$$

where we have redefined P_n as P_n-P_{nn} to absorb the $n=n'$ part of $P_{nn'}$. Equation (25) is the central result of this paper. The right hand side contains three terms. The first term is the ballistic contribution. The second term is the scatter-out term due to diffuse scattering. Moreover, the third term is the scatter-in term or the vertex corrections. Below, we will apply it to several problems and compare the results to experiments.

IV. BARRIER THICKNESS DEPENDENCE WITH DEFECT SCATTERING

The solution of Eq. (25) for a barrier of thickness t is

$$\rho_n(z)=\sum_m A_{nm}e^{-\lambda_m z}, \tag{26}$$

where λ_m are the eigenvalues of the matrix M whose elements are

$$M_{nn'}=(2\kappa_n+P_n)\delta_{nn'}-P_{nn'}(1-\delta_{nn'}). \tag{27}$$

M is diagonalized by matrix A whose elements are A_{nm}.

Suppose that λ_0 is the smallest eigenvalue. For thick barriers and $(\lambda_n-\lambda_0)z\gg 1$ for all $n\neq 0$, the solution simplifies to

$$\rho_n(z)=A_{n0}e^{-\lambda_0 z}. \tag{28}$$

Applying first-order perturbation theory to Eq. (25), we find $\lambda_n=2\kappa_n+P_n$ and

$$A_{n0}=\frac{A_{00}P_{n0}}{\lambda_n-\lambda_0}. \tag{29}$$

The scatter-out (P_n) contribution represents a simple renormalization of the decay wave vector from $2\kappa_n$ to λ_n. The scatter-in term (vertex corrections) has a much more dramatic effect. Through Eq. (28), it makes all states decay at the same decay rate λ_0. For clean barriers, $A_{n0}\ll A_{00}$.

A good test of our model is the comparison to the recent measurements of tunneling resistance for single crystal Fe/MgO/Fe magnetic tunnel junctions.[6,10] These measurements provide two sets of resistance for the same barrier layer, R_P when the moments of the two Fe electrodes are aligned parallel (P) and R_{AP} when they are antiparallel (AP). The parallel resistance R_P is dominated by the majority Δ_1 band.[4] The conductance is proportional to the transmitted charge density, $\rho_0(t)$, at $z=t$. The thickness dependence of R_P is

$$R_P=R_0e^{(2\kappa_0+P_0)t}, \tag{30}$$

where $R_0=h/(Ae^2A_{00})$ with A being the area of the sample. Because the Fe minority-spin channel does not have the Δ_1 band at the Fermi energy, the dominant contribution to the antiparallel resistance R_{AP} is the vertex correction term to the Δ_2, $\Delta_{2'}$, and Δ_5 bands[4] due to the scattering from the Δ_1 majority-spin band from the incident Fe electrode, represented by A_{n0} in Eq. (29), which yields

$$R_{AP}=\frac{h}{Ae^2}\frac{e^{(2\kappa_0+P_0)t}}{\Sigma_n v_nA_{n0}/v_0}=\frac{\eta R_0}{P}e^{(2\kappa_0+P_0)t}, \tag{31}$$

where $\eta=v_0P/\Sigma_{n\neq 0}[v_nP_{n0}/(\lambda_n-\lambda_0)]$ (with $P=\Sigma_nP_{n0}$) is assumed to be a constant independent of the scattering rates and v_n is the z component of the velocity of band n inside the electrodes. Taking the ratio of Eqs. (30) and (31), we find $P=\eta R_P/R_{AP}$ or

$$\frac{R_P}{R_{AP}}=\sum_{n\neq 0}\frac{v_nP_{n0}}{v_0(\lambda_n-\lambda_0)}. \tag{32}$$

This is a significant result because it directly links the TMR (R_{AP}/R_P-1 for the optimistic definition) to the vertex corrections due to P_{n0}. Because for a typical junction $R_P<R_{AP}$, the key for raising TMR (reducing the ratio R_P/R_{AP}) is to reduce the scattering rates P_{n0}.

By combining Eqs. (30) and (31), we find

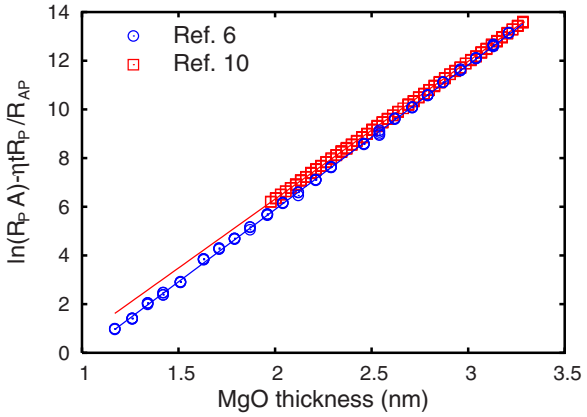

FIG. 2. (Color online) Resistance of Fe/MgO/Fe junctions. $\ln(R_P A) - \eta t R_P/R_{AP}$ versus MgO thickness t. Experimental data are from Ref. 6 (blue circle) and Ref. 10 (red square) and the fitted lines are $\ln(R_0 A) + 2\kappa_0 t$.

$$\ln(R_P) - \eta t R_P/R_{AP} = \ln(R_0) + 2\kappa_0 t. \tag{33}$$

This leaves three adjustable parameters, η, κ_0, and R_0, to fit with experiments.

In Fig. 2, we fit Eq. (33) to the measurements of Refs. 6 and 10. For the data set from Ref. 6, the fitted parameters are $\kappa_0 = 2.97\ \text{nm}^{-1}$, $\eta = 1.86\ \text{nm}^{-1}$, and $R_0 A = 0.0025\ \Omega\ \mu\text{m}^2$. For the data set from Ref. 10, because there is no curvature in the original $\ln R_P$ or $\ln R_{AP}$ versus MgO thickness plot, there is no constraint on the value of η. Therefore, we fix its value at $\eta = 1.86\ \text{nm}^{-1}$ as fitted from the data set of Ref. 6. Then, the other parameters are fitted to be $\kappa_0 = 2.83\ \text{nm}^{-1}$ and $R_0 A = 0.0067\ \Omega\ \mu\text{m}^2$. There are very good agreements in κ_0 between the two sets of data and with the first-principles value $\kappa_0 = 2.92\ \text{nm}^{-1}$.

The scattering rates, $P = \eta R_P/R_{AP}$ (scatter in) and $P_0 = \lambda_0 - 2\kappa_0$ (scatter out), are plotted in Fig. 3. To obtain λ_0 for each sample, we first plot $\log(R_P R_{AP})/2$ versus t and find the linear fit,

$$\frac{1}{2}\ln(R_P R_{AP}) = \lambda_0 t + L_0, \tag{34}$$

where the average decay rate for all data is found to be $\lambda_0 = 6.5\ \text{nm}^{-1}$ for Ref. 6 and $\lambda_0 = 6.13\ \text{nm}^{-1}$ for Ref. 10. Then, for each sample, we use $\lambda_0 t = \ln(R_P R_{AP})/2 - L_0$ to find its λ_0. Although in our model we do not require $P = P_0$, from Fig. 3, it is clear that the two scattering rates are essentially the same. We also see that for barrier thickness less than 1.6 nm, the scattering rate is very high. Above 1.6 nm, the scattering rate is nearly a constant, at about $0.5\ \text{nm}^{-1}$, which corresponds to an effective scattering length of 2 nm. The samples with a higher TMR (Ref. 10) have a correspondingly lower scattering rate.

Now, we can give another reason why we think that the agreement in Fig. 1 between the first-principles R_P and experiments is probably accidental. If Eq. (2) is the correct expression for the resistance even in the presence of diffusive scattering, then the relevant quantity in the exponential should be $2\kappa_0$. The difference between λ_0 and $2\kappa_0$ would

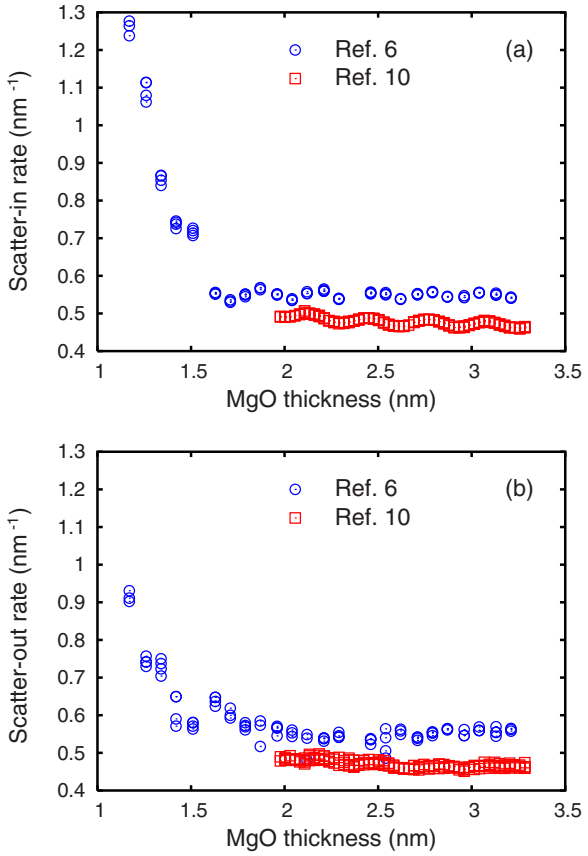

FIG. 3. (Color online) Scattering rate of Fe/MgO/Fe junctions using experimental data from Ref. 6 (blue circle) and Ref. 10 (red square). (a) The scatter-in rate, $P = \eta R_P/R_{AP}$. (b) The scatter-out rate, $P_0 = \lambda_0 - 2\kappa_0$.

simply arise from fitting a polynomial over a finite range with an exponential and should have no physical meaning. This difference, which defines P_0, agrees nearly perfectly with the scattering term P. It suggests that P_0 reflects real physics; thus, Eq. (2) is not a valid description of the tunneling resistance in the presence of diffusive scattering.

Oxygen vacancies in MgO are a major source of defect scattering.[16] The effect of defect scattering within the MgO layer is modeled in the layer-KKR calculation with vacancies on the oxygen sites varied between 0% and 1% by using the coherent-potential approximation.[17] The calculation yields an increase of the decay wave vector by $P_0/2 = 0.28\ \text{nm}^{-1}$ when the vacancy concentration reaches 0.5%. Therefore, a very small amount of oxygen vacancies within the MgO layer can account for the observed diffusive scattering effect.

V. INTERFERENCE OF EVANESCENT STATES

The second validation of our model is that the oscillatory TMR due to the interference between evanescent states is independent of the barrier thickness. This is the direct consequence that all evanescent states should have the same thickness dependence in the presence of nonspecular scattering and agrees with the measured oscillatory term in the tunneling current.[6,10] The existence of the interference be-

tween evanescent states in magnetic tunnel junctions was predicted by first-principles calculations.[4] However, the specular transmission calculated from first-principles predicts a much faster decay of the interference term than the total current, which is in disagreement with the experiments. Vertex corrections account for this discrepancy.

The interference occurs due to the presence of two tunneling states at certain $\mathbf{k}_\parallel$ at the Fermi energy. The two states have complex wave vectors along the z direction, with different real parts and the same imaginary part,[4] in the form $k_{1(2)}=k^r_{1(2)}+i\kappa_1$, with 1 and 2 labeling the two states. In this case, we consider both states together as a single effective tunneling channel and label such a channel with a subscript 1. The electron density at position z from the linear combination of both states in the absence of nonspecular scattering is

$$\rho_1^{(0)}(z) = 2e^{-2\kappa_1 z}[1 + \alpha\cos(qz + \phi)], \tag{35}$$

where $q=k^r_1-k^r_2$, $\alpha<1$ accounts for partial incoherence between the two wave functions, and ϕ is the initial phase difference between them. Accordingly, the ballistic term in the master equation [Eq. (25)] for the density $\rho_1(z)$ is also modified with an additional interference term,

$$\frac{d\rho_1(z)}{dz} = \left[-\lambda_1 - \frac{q\alpha\sin(qz+\phi)}{1+\alpha\cos(qz+\phi)}\right]\rho_1(z) + P_{10}\rho_0(z), \tag{36}$$

where P_{10} is the scattering rate from the Δ_1 state at $\mathbf{k}_\parallel=0$ (labeled by the subscript 0) into the channel ρ_1, and we have neglected all other scatter-in terms. The main tunneling channel ρ_0 is unaffected by the interference effect off the normal direction, so ρ_0 is still given by Eq. (28) with $n=0$. The approximate solution to Eq. (36) is

$$\rho_{\mathbf{k}_\parallel}(z) \approx \frac{P_{10}A_{00}e^{-\lambda_0 z}}{\lambda_1-\lambda_0}[1+\beta\cos(qz+\phi+\phi')], \tag{37}$$

where $\beta=\alpha q/\sqrt{(\lambda_1-\lambda_0)^2+q^2}$ and $\tan\phi'=-q/(\lambda_1-\lambda_0)$. Thus, in the presence of nonspecular scattering, the magnitude of the oscillatory interference term scales with the barrier thickness at the same rate as the total current.

By using 66 048 $\mathbf{k}_\parallel$ points for the entire 2DBZ in the layer-KKR calculation, we find that for a large portion of the 2DBZ in the minority-spin channel in the parallel configuration, as well as both spin channels for the antiparallel configuration, the transmission is an oscillatory function of the barrier thickness. By calculating the complex band structure of MgO(001) within the energy gap at the Fermi level of the Fe electrode, we find for each $\mathbf{k}_\parallel$ point the wave vector q for this oscillation. The average value for q is 7.0 nm^{-1}. For the entire 2DBZ, no values of q exceed 14 nm^{-1}.

We now compare our calculation to the experiment. Due to the small thickness range (about 1 nm) and large noise in the experimental data, it is difficult to extract reliable value of the oscillation period. Reference 10 used a fit with multiple periods, on top of a polynomial background to extract two periods, 3.2 and 9.9 Å. Here, we extract the Fourier components from their data by using the following procedure. The data are first scaled by $\exp(-\lambda_0 t)$ to remove the exponential factor, then a constant is subtracted to obtain a zero average. The resulting data are repeated to form a periodic function with period T_m, where T_m is greater than the thickness range of the original data. To avoid introducing an artificial Fourier component due to T_m, we average over many values of T_m, which is varied by inserting additional data points with zero value at thicknesses outside the experimental data range.

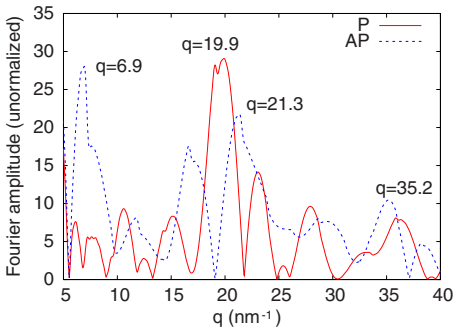

FIG. 4. (Color online) Fourier transform of the tunneling resistance (Ref. 10) scaled by $e^{-\lambda_0 t}$ with $\lambda_0=6.13$ nm^{-1} for P (red solid curve) and AP (blue dashed curve) configurations.

Figure 4 shows the Fourier transform of the data of Ref. 10 scaled by $\exp(-\lambda_0 t)$ for both P and AP configurations. The value for λ_0 is chosen from the fit in Fig. 2, $\lambda_0=2\kappa_0+P_0=6.13$ nm^{-1}. The Fourier peak at $q=6.9$ nm^{-1} in the AP spectrum is in excellent agreement with the calculated value of $q=7.0$ nm^{-1}. The period corresponding to this peak is 9.1 Å in good agreement with 9.9 Å found by Ref. 10. However, this peak is not robust against small variations of λ_0 and T_m. The reason is that this period is almost the total range of the data set (1.2 nm). Thus, it is not surprising that the same peak does not show up in the P spectrum.

The 3 Å period oscillation observed in Refs. 6 and 10 corresponds to the Fourier peaks at $q=19.9$ nm^{-1} (P) and $q=21.3$ nm^{-1} (AP). Noting that the first-principles calculation does not predict any interference peaks near this value, we argue that this period is a secondary effect. Indeed, in the AP case, the two peaks at $q=21.3$ nm^{-1} and 35.2 nm^{-1} are almost exactly $2\pi/a\pm6.9$ nm^{-1}, with $a=0.221$ nm as the lattice spacing of the MgO layers. Thus, these two peaks result from the product of a $q=6.9$ nm^{-1} oscillatory factor and an additional factor with a period of a single MgO monolayer. The monolayer period oscillation most likely arises from the interface roughness damping of the interference. One possibility, for example, is that the interference effect can be significantly damped near the step edges.

VI. DIFFUSE SCATTERING ON THE INTERFACE

Finally, we apply our model to another source of nonspecular scattering, which is the scattering of the transmitted waves outside the barrier layer near the interface. In the case of the AP alignment, the incident majority Δ_1 wave function has the largest electron density on the exit side of the interface. This wave function continues to exponentially decay into the minority-spin channel of the exit side electrode,

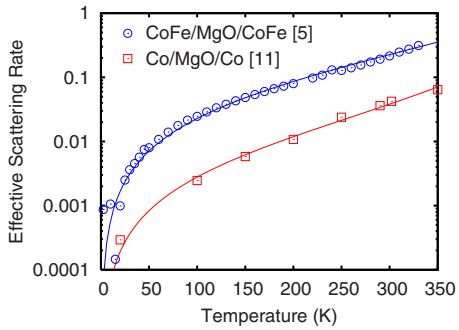

FIG. 5. (Color online) Dimensionless effective scattering rate $\xi(T)$ in the interface region as a function of the temperature for CoFe/MgO/CoFe (Ref. 5) (blue circle) and Co/MgO/Co (Ref. 11) (red box) junctions. Solid curves are fits with Eq. (41).

which does not have a Δ_1 band. Without nonspecular scattering, the Δ_1 band does not contribute to the AP current, leading to the theoretically predicted TMR of over 6000%.[4,18] The nonspecular scattering from the evanescent Δ_1 band into the Fe minority Bloch states can greatly increase the AP current and reduce the TMR. By dropping the ρ_n term on the right hand side of Eq. (25), we have

$$\frac{d\rho_n(z)}{dz} = P'_{n0}A_{00}e^{-\lambda_0 t - 2\kappa'(z-t)}, \tag{38}$$

where κ' is the decay rate of the evanescent Δ_1 wave function in the minority channel and P'_{n0} is the scattering rate from the Δ_1 state into state n. By integrating, we find

$$\rho_n(z \to \infty) = \left(\frac{P_{n0}}{\lambda_n - \lambda_0} + \frac{P'_{n0}}{2\kappa'}\right)A_{00}e^{-\lambda_0 t}. \tag{39}$$

This leads to a modification of R_{AP} in Eq. (31) due to P'_{n0}. Because R_P measured in experiments is mostly independent of temperature, we can assume that for these samples, P in Eq. (30) is independent of temperature. This is consistent with the assumption that P is mostly due to scattering centers such as oxygen vacancies inside the barrier layer. The temperature dependence of R_{AP} is only through P'_{n0} and yields

$$\frac{1}{R_{AP}(T)} = \frac{1}{R_{AP}(0)} + \frac{\xi(T)}{R_P(0)}, \tag{40}$$

where $\xi(T) = \Sigma_n(v_n P'_{n0}/2v_0\kappa')$ is a dimensionless effective scattering rate. Because most scattering mechanisms increase the scattering rate with the temperature, $\xi(T)$ should increase with the temperature, which causes a decrease of R_{AP} with the temperature. The temperature dependence of $\xi(T)$ provides clues to the scattering mechanism near the interfaces.

A nearly temperature-independent R_P and a decreasing R_{AP} with temperature are consistent with experiments.[5,11] In Fig. 5, we plot $\xi(T)$ as a function of the temperature for two junctions: a CoFe/MgO/CoFe junction[5] and a Co/MgO/Co junction.[11] The scattering rate for both samples fit the following temperature dependence:

$$\xi(T) = a\left(\frac{T}{T_0 - T}\right)^{3/2}, \tag{41}$$

with $a=0.31$ and $T_0=670$ K for CoFe/MgO/CoFe and $a=0.024$ and $T_0=520$ K for Co/MgO/Co. We note that Ref. 19 obtained a $T^{3/2}$ low temperature dependence of electron-magnon scattering rate for a nearly half-metallic ferromagnet, between a propagating state in one spin channel and a localized state in the other. Here, the situation may be similar; thus the appearance of a $T^{3/2}$ temperature dependence may not be surprising. Complete analysis of this temperature dependence is beyond the scope of this paper and will be considered in future works.

An effective inverse scattering length can be calculated from $2\kappa'\xi(T)$. The layer-KKR calculation yields $\kappa' = 10.7$ nm^{-1} for bcc Fe and $\kappa' = 12.4$ nm^{-1} for bcc Co, both using the same lattice constant of 2.866 Å. By scaling the scattering rates at room temperature in Fig. 5 by $2\kappa'$, we find an effective scattering rate of about 6 nm^{-1} for MgO/CoFe interface and about 1 nm^{-1} for MgO/Co interface. These values correspond to an effective mean free path of about 1.7 Å for MgO/CoFe interface and about 10 Å for MgO/Co interface.

VII. CONCLUSION

In conclusion, we have derived a master equation [Eq. (25)] to account for the vertex corrections due to diffusive impurity scattering inside the barrier layer of a magnetic tunnel junction. Our model can also be used to study the effects of nonspecular scattering in the interface regions. The model yields excellent agreement with experiments in the barrier thickness dependence of the resistance and oscillatory TMR. The interface scattering has been analyzed to yield additional insight in the experimental data, in particular, the temperature dependence of interface scattering.

It is worth emphasizing again the significance of Eq. (32). This result and the accompanying analysis of the experimental data indicate that the nonspecular scattering in the MgO layer and at the interfaces has become the bottleneck for improving the performance of the magnetic tunnel junctions. Reducing this effect by eliminating lattice defects inside the MgO layer, and improving the quality of the interfaces, is the key for achieving giant TMR.

ACKNOWLEDGMENTS

We thank S. S. P. Parkin, S. Yuasa, and Y. Suzuki for providing their original experimental data from Refs. 5, 6, 10, and 11. This research was conducted at the Center for Nanophase Materials Sciences, which is sponsored at the Oak Ridge National Laboratory by the Division of Scientific User Facilities, U.S. Department of Energy. It was also supported by the State Key Project of Fundamental Research of the Ministry of Science and Technology (No. 2006CB932200), National Natural Science Foundation of China (No. 10574156, No. 50325104, and No. 50721001), and the Knowledge Innovation Program project of Chinese Academy of Sciences.

*xgz@ornl.gov

[1] M. Julliere, Phys. Lett. **54A**, 225 (1975).
[2] T. Miyazaki and N. Tezuka, J. Magn. Magn. Mater. **139**, L231 (1995).
[3] J. S. Moodera, L. R. Kinder, T. M. Wong, and R. Meservey, Phys. Rev. Lett. **74**, 3273 (1995).
[4] W. H. Butler, X.-G. Zhang, T. C. Schulthess, and J. M. MacLaren, Phys. Rev. B **63**, 054416 (2001).
[5] S. S. P. Parkin, C. Kaiser, A. Panchula, P. M. Rice, B. Hughes, M. Samant, and S.-H. Yang, Nat. Mater. **3**, 862 (2004).
[6] S. Yuasa, T. Nagahama, A. Fukushima, Y. Suzuki, and K. Ando, Nat. Mater. **3**, 868 (2004).
[7] John G. Simmons, J. Appl. Phys. **34**, 1793 (1963).
[8] J. C. Slonczewski, Phys. Rev. B **39**, 6995 (1989).
[9] D. Bagrets, A. Bagrets, A. Vedyayev, and B. Dieny, Phys. Rev. B **65**, 064430 (2002).
[10] R. Matsumoto, A. Fukushima, T. Nagahama, Y. Suzuki, K. Ando, and S. Yuasa, Appl. Phys. Lett. **90**, 252506 (2007).
[11] S. Yuasa, A. Fukushima, H. Kubota, Y. Suzuki, and K. Ando, Appl. Phys. Lett. **89**, 042505 (2006).
[12] J. M. MacLaren, X.-G. Zhang, W. H. Butler, and Xindong Wang, Phys. Rev. B **59**, 5470 (1999).
[13] Christian Heiliger, Peter Zahn, and Ingrid Mertig, in *Magnetic Thin Films, Heterostructures, and Device Materials*, edited by C. Ross, MRS Symposia Proceedings Vol. 941E (Materials Research Society, Warrendale, PA, 2006), p. 0941-Q03-05.
[14] X.-G. Zhang, Zhong-Yi Lu, and Sokrates T. Pantelides, Appl. Phys. Lett. **89**, 032112 (2006).
[15] X.-G. Zhang and W. H. Butler, Phys. Rev. B **51**, 10085 (1995).
[16] J. P. Velev, K. D. Belashchenko, S. S. Jaswal, and E. Y. Tsymbal, Appl. Phys. Lett. **90**, 072502 (2007).
[17] J. S. Faulkner and G. M. Stocks, Phys. Rev. B **21**, 3222 (1980).
[18] X.-G. Zhang and W. H. Butler, Phys. Rev. B **70**, 172407 (2004).
[19] Xindong Wang and X.-G. Zhang, Phys. Rev. Lett. **82**, 4276 (1999).